
ExactDreamer: High-Fidelity Text-to-3D Content Creation via Exact Score Matching

Yumin Zhang^{1*} Xingyu Miao^{2*} Haoran Duan^{1*}
Bo Wei¹ Tejal Shah¹ Yang Long² Rajiv Ranjan¹

¹Newcastle University, UK ²Durham University, UK

Abstract

Text-to-3D content creation is a rapidly evolving research area. Given the scarcity of 3D data, current approaches often adapt pre-trained 2D diffusion models for 3D synthesis. Among these approaches, Score Distillation Sampling (SDS) has been widely adopted. However, the issue of over-smoothing poses a significant limitation on the high-fidelity generation of 3D models. To address this challenge, LucidDreamer replaces the Denoising Diffusion Probabilistic Model (DDPM) in SDS with the Denoising Diffusion Implicit Model (DDIM) to construct Interval Score Matching (ISM). However, ISM inevitably inherits inconsistencies from DDIM, causing reconstruction errors during the DDIM inversion process. This results in poor performance in the detailed generation of 3D objects and loss of content. To alleviate these problems, we propose a novel method named Exact Score Matching (ESM). Specifically, ESM leverages auxiliary variables to mathematically guarantee exact recovery in the DDIM reverse process. Furthermore, to effectively capture the dynamic changes of the original and auxiliary variables, the LoRA of a pre-trained diffusion model implements these exact paths. Extensive experiments demonstrate the effectiveness of ESM in text-to-3D generation, particularly highlighting its superiority in detailed generation. Code is available at: <https://github.com/zymvszym/ExactDreamer>.

1 Introduction

3D content creation plays a crucial role across multiple domains such as virtual and augmented reality, game design, head modeling, and more. Among these, text-to-3D generation allows for the synthesis of imaginative 3D models guided by text captions and has become a burgeoning research area in recent years. Despite the significant advancements brought about by deep learning techniques, previous methods [1, 40, 4, 5] are limited by the scarcity of 3D data.

Benefiting the advantages of diffusion models [7, 35], which have achieved remarkable progress in Text-to-Image (T2I) [30, 32], recent works attempt to incorporate pre-trained T2I diffusion models into the text-to-3D generation task, aiming to synthesize high-fidelity 3D models without relying on extensive 3D datasets [18, 25]. In this research area, Score Distillation Sampling (SDS) proposed in DreamFusion [23] has been widely adopted due to its impressive generation quality.

However, as indicated in [17, 38], issues such as over-smoothing hinder the generation of detailed, high-fidelity 3D models. Various works have been proposed to address the limitations of SDS. For instance, ProlificDreamer [38] treats the modeled 3D parameters as random variables and thus proposes Variational Score Distillation (VSD), achieving a better balance between high-fidelity and diversity results. However, the long training time required for VSD is a significant drawback.

*Equal contribution



Figure 1: **Text-to-3D samples generated from our framework.** We propose a novel method named Exact Score Matching (ESM) that utilizes the pre-trained 2D diffusion model to guide high-fidelity content generation. The generative 3D results illustrate the superiority of ESM.

From another perspective, LucidDreamer [17] introduces Interval Score Matching (ISM), employing Denoising Diffusion Implicit Models (DDIM) [34] to mitigate the over-smoothing caused by the averaging effect during the 3D generation process, and the experimental results demonstrate ISM can synthesis competitive 3D models within a short time. Nevertheless, as mentioned in [6], DDIM is unstable in many cases. The encoding process from realistic samples to noise vectors and the reverse often results in inexact reconstructions, leading to inconsistent generation.

Considering the realistic requirement of generating 3D models within a limited time, we propose a novel method named Exact Score Matching (ESM) based on ISM, which focuses on alleviating the inconsistencies in the DDIM process and enhancing high-fidelity content generation. Specifically, we

first illustrate how the inherent bias in ISM can be alleviated by releasing the assumption of local linear approximation. Inspired by recent research [37], we introduce auxiliary noise variables that facilitate exact recovery during DDIM processes. To effectively merge these auxiliary noise variables with the original noise variables, we employ an interactive recovery path. This path is implemented by the Low-rank Adaptation (LoRA) [8, 31] of a pre-trained 2D diffusion model, which also serves to adaptively capture the dynamic changes of these integrated variables. Overall, our main contributions can be summarized as follows:

- We analyze the local linear approximation in DDIM, which hinders the detailed 3D model generation. Based on this, we propose a novel text-to-3D method named ESM, aiming to construct an exact recovery and thus enhance the consistencies of 3D model generation.
- By utilizing auxiliary noise variables, ESM constructs an exact recovery strategy. Besides, the LoRA is leveraged to capture the dynamic change of the original and auxiliary noise variables effectively and adaptively.
- We conduct extensive experiments, and the results demonstrate the effectiveness of ESM, particularly in generating high-fidelity and detailed models.

2 Related Work

2.1 Diffusion models

Diffusion models [7, 35] have become the dominant method in image generation and have shown potential for application in 3D generation. Generally, based on the types of 3D data, diffusion models have been widely applied across various 3D representations, such as NeRF [20], Gaussian Splatting [13], point clouds, and others. For example, [19, 43] generate the point clouds using diffusion algorithms. Point-E [22] first uses a T2I diffusion model to generate images, which are then used as conditions for the second step of 3D point cloud synthesis. Additionally, Shape-E [12] is proposed to generate the NeRF representation of 3D objects, and the Gaussian splatting is adapted as a generative setting in DreamGaussian [36]. Due to the impressive performance of Gaussian splatting on 3D models, our work adopts it as the 3D learnable representation.

2.2 Text-to-Image Generation

Impressive achievements have been made in the field of T2I generation. Early works can be mainly grouped into GAN-based [27, 42, 41, 16] and autoregressive-based [26, 3, 39] methods, which are limited to small-scale datasets and sequential error accumulation, respectively. More recently, methods [21, 28, 32] integrating diffusion models into T2I have achieved state-of-the-art performance. Among them, the first work GLIDE [21] replaces the original class label with text, thus achieving text-guided generation. Following GLIDE, Imagen [32] adopts a pre-trained language model as the text encoder. Moreover, diffusion-based methods are also emerging in some highly relevant areas, such as text-guided art generation [29, 11, 9] and text-guided image editing [14, 15].

2.3 Text-to-3D Generation

To generate the 3D content guided by the text prompts, current text-to-3D methods typically utilize differentiable rendering techniques to obtain images aligned with the text. For example, DreamField [10] combines NeRF [20] with a pre-trained CLIP [24] model to achieve text-to-3D generation. DreamFusion [23] proposes the score distillation sampling (SDS) loss with volumetric representations used in NeRF to generate high-fidelity 3D content. Further, based on the SDS, Magic3D [18] introduces a coarse-to-fine optimization approach, starting with a coarse representation and then refining the 3D mesh model using differentiable rendering and SDS. In a similar two-stage manner, Fantasia3D [2] utilizes DMTet [33] to obtain geometric knowledge and proposes a bidirectional reflectance distribution function to model the appearance. Besides, aiming to address the over-smoothing in SDS-based methods, ProlificDreamer [38] introduces variational score distillation (VSD) treating the input prompt as a random variable rather than a constant. LucidDreamer combines interval score matching (ISM) with DDIM [34] to mitigate over-smoothing caused by naive averaging. However, the local linear approximation in the DDIM inversion process results in instability during

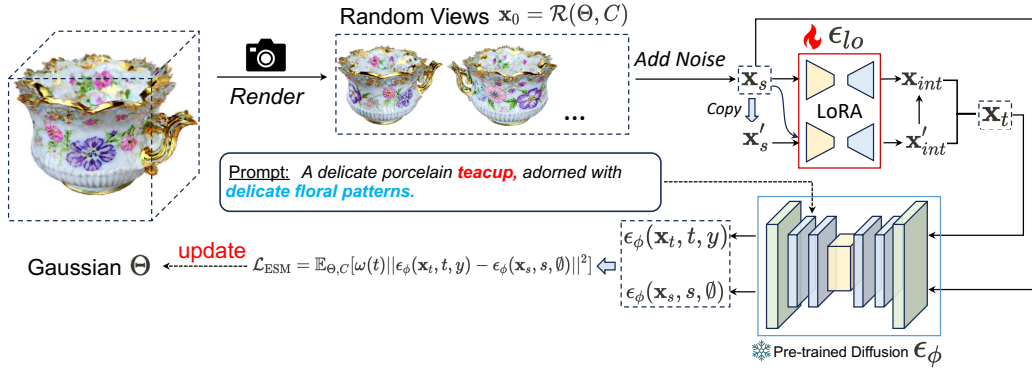


Figure 2: **Overview of our framework.** Under the camera pose C , the Gaussian Splatting Θ is rendered to 2D image $\mathbf{x}_0 = \mathcal{R}(\Theta, C)$ and then approach to \mathbf{x}_s via DDIM inversion. To construct the exact recovery path, we introduce an auxiliary variable \mathbf{x}'_s that is copied from \mathbf{x}_s . Intermediate variables \mathbf{x}_t and \mathbf{x}'_t are estimated by the LoRA, and then mixed to obtain \mathbf{x}_t . Finally, Θ is updated via optimizing \mathcal{L}_{ESM} calculated by \mathbf{x}_s and \mathbf{x}_t .

the generation in many cases [6]. To address the inconsistencies caused by this approximation, we introduce auxiliary variables to construct an exact recovery path.

3 Methodology

In this section, we first review the preliminaries of 3D Learnable Representations, the DDIM inversion process, and ISM (see Section 3.1), which are foundational for our exploration. We then introduce our proposed method, Exact Score Matching (ESM), based on ISM. Specifically, our main contribution is addressing the inherent bias in DDIM by introducing auxiliary variables to design an exact inversion process. Considering that the noise latent changes during the optimization process, we utilize LoRA to adaptively model these dynamic changes (see Section 3.2). Additionally, we analyze the differences between ISM and ESM (see Section 3.3). The overview of our method is shown in Figure 2.

3.1 Preliminaries

3.1.1 3D Learnable Representations

Existing text-to-3D generation works that primarily incorporate NeRF [20] have shown that rendering resolution and batch size settings during the training process significantly influence the quality of the final 3D creation. Considering the substantial computational resources required by increasing rendering resolution, we adopt 3D Gaussian Splatting [13], an efficient explicit rendering method, for both rendering and optimization as the 3D representation. Specifically, given a learnable 3D representation Θ , the differentiable rendering function $\mathcal{R}(\Theta, C)$ can be defined to render an image under the camera pose C .

3.1.2 Review of DDIM inversion

The DDIM inversion sampling scheme proposed in [34] can be formulated as follows:

$$\mathbf{x}_t = \sqrt{\bar{\alpha}_t} \left(\frac{\mathbf{x}_{t-1} - \sqrt{1 - \bar{\alpha}_{t-1}} \epsilon_\phi(\mathbf{x}_{t-1}, t, \emptyset)}{\sqrt{\bar{\alpha}_{t-1}}} \right) + \sqrt{1 - \bar{\alpha}_t - \sigma_t^2} \epsilon_\phi(\mathbf{x}_t, t, \emptyset) + \sigma_t z^*, \quad (1)$$

where $\bar{\alpha} = \prod_{i=1}^t \alpha_i$, and α_i is the predefined constant of the timestep i , and z^* is the white noise. We use the \mathbf{x}_{t-1} and \mathbf{x}_t to denote the noisy latent, $\epsilon_\phi(\mathbf{x}_t, t, \emptyset)$ is modeled by the pretrained neural network ϕ with the unconditioned \emptyset . When the hyperparameter σ^2 is set as $(1 - \alpha_t)(1 - \bar{\alpha}_{t-1}) / (1 - \bar{\alpha}_t)$, the DDIM is equivalent to DDPM [7]. To accelerate the sampling process, DDIM set the $\sigma^2 = 0$, and the \mathbf{x}_t can be approximately predicted from \mathbf{x}_{t-1} as follows:

$$\begin{aligned}
\mathbf{x}_t &= \sqrt{\bar{\alpha}_t} \left(\frac{\mathbf{x}_{t-1} - \sqrt{1 - \bar{\alpha}_{t-1}} \epsilon_\phi(\mathbf{x}_t, t, \emptyset)}{\sqrt{\bar{\alpha}_{t-1}}} \right) + \sqrt{1 - \bar{\alpha}_t} \epsilon_\phi(\mathbf{x}_t, t, \emptyset) \\
&\approx \sqrt{\bar{\alpha}_t} \left(\frac{\mathbf{x}_{t-1} - \sqrt{1 - \bar{\alpha}_{t-1}} \epsilon_\phi(\mathbf{x}_{t-1}, t, \emptyset)}{\sqrt{\bar{\alpha}_{t-1}}} \right) + \sqrt{1 - \bar{\alpha}_t} \epsilon_\phi(\mathbf{x}_{t-1}, t, \emptyset).
\end{aligned} \tag{2}$$

Such approximation relies on the linear assumption $\epsilon_\phi(\mathbf{x}_t, t, \emptyset) \approx \epsilon_\phi(\mathbf{x}_{t-1}, t, \emptyset)$. However, as indicated in [37], this approximation results in the propagation of errors and thus leads to inconsistent loss in both forward and reverse processes.

Algorithm 1 Exact Score Matching (ESM)

Initialization: DDIM inversion step size δ_T and δ_S , the target prompt y , and the mixture ratio ρ
while Θ is not converged **do**
 Sample: $\mathbf{x}_0 = \mathcal{R}(\Theta, C)$, $t \sim \mathcal{U}(1, 1000)$
 let $s = t - \delta_T$, $n = s / \delta_S$
 for $i = [1, \dots, n]$ **do**
 $\mathbf{x}_{i\delta_s} = \sqrt{\bar{\alpha}_i} \left(\frac{\mathbf{x}_{(i-1)\delta_s} - \sqrt{1 - \bar{\alpha}_{i-1}} \epsilon_\phi(\mathbf{x}_{i\delta_s}, i\delta_s, \emptyset)}{\sqrt{\bar{\alpha}_{i-1}}} \right) + \sqrt{1 - \bar{\alpha}_i} \epsilon_\phi(\mathbf{x}_{i\delta_s}, i\delta_s, \emptyset)$
 end for
 Copy a latent variable \mathbf{x}'_s from \mathbf{x}_s , and parameterize ϵ_{lo} by a LoRA.
 Let $\mathbf{x}_s \rightarrow \mathbf{x}_{int}$, $\mathbf{x}'_s \rightarrow \mathbf{x}'_{int}$ via
 $\mathbf{x}'_{int} = \sqrt{\bar{\alpha}_t} \left(\frac{\mathbf{x}'_s - \sqrt{1 - \bar{\alpha}_t} \epsilon_{lo}(\mathbf{x}_s, s, \emptyset)}{\sqrt{\bar{\alpha}_s}} \right) + \sqrt{1 - \bar{\alpha}_t} \epsilon_{lo}(\mathbf{x}_s, s, \emptyset)$
 $\mathbf{x}_{int} = \sqrt{\bar{\alpha}_t} \left(\frac{\mathbf{x}_s - \sqrt{1 - \bar{\alpha}_t} \epsilon_{lo}(\mathbf{x}'_{int}, s, \emptyset)}{\sqrt{\bar{\alpha}_{int}}} \right) + \sqrt{1 - \bar{\alpha}_t} \epsilon_{lo}(\mathbf{x}'_s, s, \emptyset)$
 Obtain the mixture noisy latent $\mathbf{x}_t = \frac{1}{\rho} [\mathbf{x}_{int} - (1 - \rho) \mathbf{x}'_{int}]$
 Predict $\epsilon_\phi(\mathbf{x}_t, t, y)$ and $\epsilon_\phi(\mathbf{x}_s, s, \emptyset)$.
 3D learnable representation Θ is updated by optimizing ESM loss
 $\nabla_{\Theta} \mathcal{L}_{\text{ESM}} = \omega(t) (\epsilon_\phi(\mathbf{x}_t, t, y) - \epsilon_\phi(\mathbf{x}_s, s, \emptyset))$
end while

3.1.3 Interval Score Matching (ISM)

ISM is first introduced in Lucidreamer [17] to alleviate the issue of the over-smoothing problem introduced by the Score Distillation Sampling (SDS) [23]. Specifically, for the given prompt y , the gradient of ISM loss is defined as:

$$\nabla_{\Theta} \mathcal{L}_{\text{ISM}}(\Theta) = [\omega(t) (\epsilon_\phi(\mathbf{x}_t, t, y) - \epsilon_\phi(\mathbf{x}_s, s, \emptyset)) \frac{\partial \mathcal{R}(\Theta, C)}{\partial C}] \quad (0 < s < t), \tag{3}$$

where $\mathcal{R}(\Theta, C)$ denotes the differential rendering function that is utilized to render an image of the camera pose C . We use Θ to denote the learnable parameters of 3D representations, and $\omega(t)$ to represent a time-dependent function. The noise latent \mathbf{x}_t and \mathbf{x}_s are calculated by the DDIM inversion process. Given the DDIM inversion step size δ_T , let $s = t - \delta_T$, and suppose \mathbf{x}_0 gradually approach to \mathbf{x}_s in n steps. Hence, for each step i ($1 \leq i \leq n$), the forward diffusion process can be calculated via:

$$\begin{aligned}
\mathbf{x}_{i\delta_s} &= \sqrt{\bar{\alpha}_i} \left(\frac{\mathbf{x}_{(i-1)\delta_s} - \sqrt{1 - \bar{\alpha}_{i-1}} \epsilon_\phi(\mathbf{x}_{i\delta_s}, i\delta_s, \emptyset)}{\sqrt{\bar{\alpha}_{i-1}}} \right) + \sqrt{1 - \bar{\alpha}_i} \epsilon_\phi(\mathbf{x}_{i\delta_s}, i\delta_s, \emptyset) \\
&\approx \sqrt{\bar{\alpha}_i} \left(\frac{\mathbf{x}_{(i-1)\delta_s} - \sqrt{1 - \bar{\alpha}_{i-1}} \epsilon_\phi(\mathbf{x}_{(i-1)\delta_s}, i\delta_s, \emptyset)}{\sqrt{\bar{\alpha}_{i-1}}} \right) + \sqrt{1 - \bar{\alpha}_i} \epsilon_\phi(\mathbf{x}_{(i-1)\delta_s}, i\delta_s, \emptyset),
\end{aligned} \tag{4}$$

where δ_s denote the step size in the approaching $\mathbf{x}_0 \rightarrow \mathbf{x}_s$. Then, \mathbf{x}_t is calculated by \mathbf{x}_s via:

$$\begin{aligned}
\mathbf{x}_t &= \sqrt{\bar{\alpha}_t} \left(\frac{\mathbf{x}_s - \sqrt{1 - \bar{\alpha}_s} \epsilon_\phi(\mathbf{x}_t, t, \emptyset)}{\sqrt{\bar{\alpha}_s}} \right) + \sqrt{1 - \bar{\alpha}_t} \epsilon_\phi(\mathbf{x}_t, t, \emptyset) \\
&\approx \sqrt{\bar{\alpha}_t} \left(\frac{\mathbf{x}_s - \sqrt{1 - \bar{\alpha}_s} \epsilon_\phi(\mathbf{x}_s, s, \emptyset)}{\sqrt{\bar{\alpha}_s}} \right) + \sqrt{1 - \bar{\alpha}_t} \epsilon_\phi(\mathbf{x}_s, s, \emptyset).
\end{aligned} \tag{5}$$

Obviously, in the optimization of ISM, there are two approximations have been introduced which result in inconsistent loss during the diffusion processes and distortion in details.

3.2 Exact Score Matching (ESM)

3.2.1 Motivation

Since the necessary discrete computation of the underlying noise schedule, DDIM relies on the linear assumption to employ. To mitigate such approximation and enhance the consistent generation, inspired by [37], we leverage the auxiliary variables to construct an exact recovery mathematically.

Concretely, the \mathbf{x}_{t-1} can be recovered from \mathbf{x}_t via the approximation in Eq. (2). Utilizing a new variable \mathbf{x}'_t copied from \mathbf{x}_t , and then \mathbf{x}_t can be exactly recovered via:

$$\mathbf{x}_t = \sqrt{\bar{\alpha}_t} \left(\frac{\mathbf{x}_{t-1} - \sqrt{1 - \bar{\alpha}_t} \epsilon_\phi(\mathbf{x}'_t, t, \emptyset)}{\sqrt{\bar{\alpha}_{t-1}}} \right) + \sqrt{1 - \bar{\alpha}_{t-1}} \epsilon_\phi(\mathbf{x}'_t, t, \emptyset). \quad (6)$$

The same strategy can directly apply in ISM to mitigate the approximations that include two parts: $\mathbf{x}_0 \rightarrow \mathbf{x}_s$ and $\mathbf{x}_s \rightarrow \mathbf{x}_t$.

3.2.2 Optimization by ESM

As analyzed above, we can mitigate the approximations by introducing extra independent variables. However, extra variables will inevitably burden the computation, especially in multiple steps approaching $\mathbf{x}_0 \rightarrow \mathbf{x}_s$. Considering this, we only mitigate the approximation in the one step approaching $\mathbf{x}_s \rightarrow \mathbf{x}_t$ in ISM. Specifically, we first introduce \mathbf{x}'_s that is copied from \mathbf{x}_s . Then, noise intermediate latent \mathbf{x}'_{int} and \mathbf{x}_{int} can be calculated via:

$$\begin{aligned} \mathbf{x}'_{int} &= \sqrt{\bar{\alpha}_t} \left(\frac{\mathbf{x}'_s - \sqrt{1 - \bar{\alpha}_t} \epsilon_{lo}(\mathbf{x}'_s, s, \emptyset)}{\sqrt{\bar{\alpha}_s}} \right) + \sqrt{1 - \bar{\alpha}_s} \epsilon_{lo}(\mathbf{x}'_s, s, \emptyset), \\ \mathbf{x}_{int} &= \sqrt{\bar{\alpha}_t} \left(\frac{\mathbf{x}_s - \sqrt{1 - \bar{\alpha}_t} \epsilon_{lo}(\mathbf{x}'_{int}, s, \emptyset)}{\sqrt{\bar{\alpha}_s}} \right) + \sqrt{1 - \bar{\alpha}_s} \epsilon_{lo}(\mathbf{x}'_{int}, s, \emptyset). \end{aligned} \quad (7)$$

Notably, the ϵ_{lo} is implemented by the LoRA [8] of a pre-trained 2D diffusion model to effectively and adaptatively capture the noisy latent changing in the optimization process. Moreover, to alleviate the diverging optimization of \mathbf{x}_{int} and \mathbf{x}'_{int} , we interact them with a predefined ratio ρ via $\mathbf{x}_t = \frac{1}{\rho}[\mathbf{x}_{int} - (1 - \rho)\mathbf{x}'_{int}]$, ($0 < \rho \leq 1$). Then, for the given prompt y , the 3D learnable representation Θ is optimized by minimizing \mathcal{L}_{ESM} :

$$\begin{aligned} \mathcal{L}_{\text{ESM}}(\Theta) &= \mathbb{E}_{t,C}[\omega(t) \|\epsilon_\phi(\mathbf{x}_t, t, y) - \epsilon_\phi(\mathbf{x}_s, s, \emptyset)\|^2] \\ &= \mathbb{E}_{t,C}[\omega(t) (\|\epsilon_\phi(\mathbf{x}_t, t, y) - \epsilon_\phi(\mathbf{x}_{int}, t, \emptyset)\|^2 + \|\epsilon_\phi(\mathbf{x}_{int}, t, \emptyset) - \epsilon_\phi(\mathbf{x}_s, s, \emptyset)\|^2)]. \end{aligned} \quad (8)$$

Through introducing an auxiliary variable \mathbf{x}'_s copied from \mathbf{x}_s , we can get an exact recovery from \mathbf{x}_s to \mathbf{x}_t , and thus reduce the accumulate error occurs in DDIM inversion process. The algorithmic pipeline of ESM is shown in Algorithm 1.

3.3 Comparison with ISM

We now compare the differences between ISM and ESM mathematically. Specifically, the optimization goal of ESM can be viewed to mitigate the error ϵ_{ISM} :

$$\epsilon_{\text{ISM}} = \|\epsilon_\phi(\mathbf{x}_t, t, y) - \epsilon_\phi(\mathbf{x}_s, s, \emptyset)\|^2. \quad (9)$$

In our ESM, as we introduce the auxiliary variable \mathbf{x}'_s to maintain an exact recovery path, the optimization goal can be decoupled into two parts as follows:

$$\epsilon_{\text{ESM}} = \|\epsilon_\phi(\mathbf{x}_t, t, y) - \epsilon_\phi(\mathbf{x}_{int}, t, \emptyset)\|^2 + \|\epsilon_\phi(\mathbf{x}_{int}, t, \emptyset) - \epsilon_\phi(\mathbf{x}_s, s, \emptyset)\|^2, \quad (10)$$

where \mathbf{x}_{int} is calculated via Equation 7. Compared with ISM, ESM has a smaller accumulated error (i.e., $\epsilon_{\text{ESM}} < \epsilon_{\text{ISM}}$), and we show this conclusion in the follows:

Theorem 1 *In diffusion-based 3D model generation, ESM is more effective than ISM in reducing accumulated error (i.e., $\epsilon_{\text{ESM}} < \epsilon_{\text{ISM}}$), thereby enhancing the detail fidelity of 3D representations.*

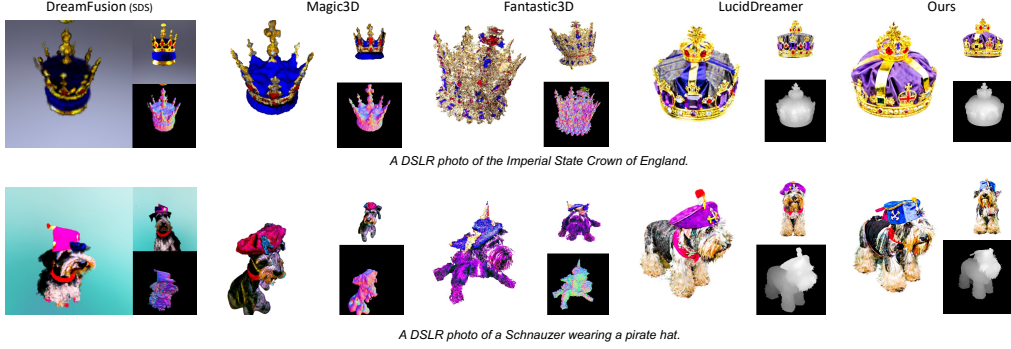


Figure 3: **Comparison with baselines in text-to-3D generation.** We compare our methods with current SoTA methods, and our method performs better in detail.

Proof: Let $\epsilon_\phi(\mathbf{x}_{int}, t, \emptyset) = \epsilon_\phi(\mathbf{x}_s, s, \emptyset) + \eta$, and we assume $0 < \eta < |\epsilon_\phi(\mathbf{x}_t, t, y) - \epsilon_\phi(\mathbf{x}_s, s, \emptyset)|$. Then ϵ_{ESM} can be represented as:

$$\begin{aligned}
 \epsilon_{\text{ESM}} &= \|\epsilon_\phi(\mathbf{x}_t, t, y) - (\epsilon_\phi(\mathbf{x}_s, s, \emptyset) + \eta)\|^2 + \|(\epsilon_\phi(\mathbf{x}_s, s, \emptyset) + \eta) - \epsilon_\phi(\mathbf{x}_s, s, \emptyset)\|^2 \\
 &= \|\epsilon_\phi(\mathbf{x}_t, t, y) - \epsilon_\phi(\mathbf{x}_s, s, \emptyset) - \eta\|^2 + \|\eta\|^2 \\
 &= \|\epsilon_\phi(\mathbf{x}_t, t, y) - \epsilon_\phi(\mathbf{x}_s, s, \emptyset)\|^2 - 2\eta\|\epsilon_\phi(\mathbf{x}_t, t, y) - \epsilon_\phi(\mathbf{x}_s, s, \emptyset)\| + 2\|\eta\|^2 \\
 &= \epsilon_{\text{ISM}} + 2\eta(\eta - \|\epsilon_\phi(\mathbf{x}_t, t, y) - \epsilon_\phi(\mathbf{x}_s, s, \emptyset)\|)
 \end{aligned} \tag{11}$$

Due to $2\eta(\eta - \|\epsilon_\phi(\mathbf{x}_t, t, y) - \epsilon_\phi(\mathbf{x}_s, s, \emptyset)\|) < 0$, hence $\epsilon_{\text{ESM}} < \epsilon_{\text{ISM}}$.

4 Experiments

4.1 Implementation details

All experimental results are implemented by using a single NVIDIA 3090 RTX GPU. The predefined parameters ρ , and $\{\delta_S, \delta_T\}$ are set as 0.93, and $\{200, 50\}$ respectively. We use the stable diffusion [28] to implement the pre-trained diffusion model ϵ_ϕ , and follow [31] to implement the LoRA. Besides, we set the training process with 5,000 iterations and leverage the pre-trained Point-E [22] to initialize the 3D gaussian splatting.

4.2 Text-to-3D Generation

The results generated by ExactDreamer are shown in Figure 1. We input various types of prompts to illustrate the robustness of our method. The results demonstrate that our method is capable of generating high-fidelity 3D models that consist of given texts, such as "a DSLR photo of a frog on a lotus leaf". Also, the photorealistic and imaginary 3D models can both be generated by ExactDreamer.

4.3 Qualitative Comparison

Utilizing the same prompt and setting in [17], we compare our method with current SoTA methods [23, 18, 2, 17]. The comparison results are shown in Figure 3. Our method, while maintaining high fidelity, is able to generate 3D models that are more consistent with the text compared to the baselines. With the prompt "A DSLR photo of the Imperial State Crown of England", our method shows significant improvement in clarity compared to DreamFusion, Magic3D, and Fantasia3D. Compared to LucidDreamer, the crown we generated is more detailed and includes a national flag. With the prompt "A DSLR photo of a Schnauzer wearing a pirate hat", our method excels in geometric shape and hair texture. Compared to LucidDreamer, the Schnauzer we generated has more detailed eyes.

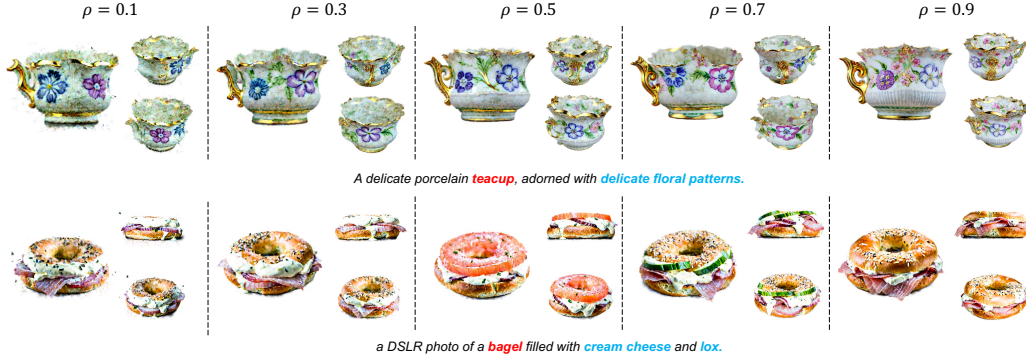


Figure 4: **Effect of mixed ratio.** We tune the ρ in the interval $\{0.1, 0.3, 0.5, 0.7, 0.9\}$. The generated results show that a higher mixed ratio is typically beneficial for high-fidelity generation.



Figure 5: **Effect of step size.** The generated results are guided by the prompt *A red motorcycle*. The parameters δ_S and δ_T are tuned in the sets $\{50, 100, 150, 200\}$ and $\{25, 50, 150, 200\}$, respectively. The results illustrate that the step sizes have a significant influence on the clarity of generated 3D objections. Obviously, higher δ_T result in blurrier results.

4.4 Parameters Exploration

As shown in Algorithm 1, the step sizes $\{\delta_T, \delta_S\}$ and mixture ratio ρ are predefined hyperparameters. In this section, we explore their effects under different settings on the final generation results.

Mixed ratio ρ The parameter ρ quantifies the relative contributions of \mathbf{x}'_{int} and \mathbf{x}_{int} . We tune the ρ within the set $\{0.1, 0.3, 0.5, 0.7, 0.9\}$ using two prompt guidance methods, and show the results in Figure 4. The results indicate that a higher ρ is beneficial for high-quality 3D model generation, whereas a lower ρ may lead to unstable optimization.

Step sizes δ_S and δ_T With the prompt of *A red motorcycle*, we tune the step sizes δ_S and δ_T within the sets $\{50, 100, 150, 200\}$ and $\{25, 50, 150, 200\}$ respectively, and present the results in Figure 5. The value of δ_S has no significant influence on the final results. Therefore, we set $\delta_S = 200$ to conserve the computational resources in the DDIM inversion process. While we mitigate the negative

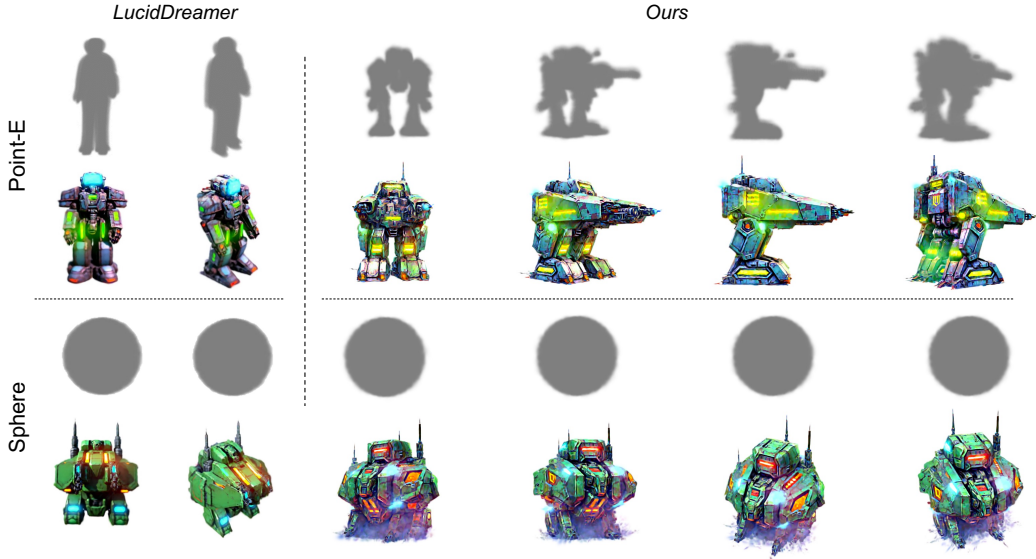


Figure 6: **Effect of different initialization.** Given the prompt "A military Mech, future, sci-fi", we compare the effect of two initialization, Point-E and Sphere, on the final generated results. The results illustrate that Point-E provides better performance, producing more geometrically detailed models. Additionally, when compared with results generated by LucidDreamer, our method demonstrates a clear advantage in detail and overall quality.

effects caused by the linear approximation, an increasing δ_T results an increasing accumulative error between \mathbf{x}_s and \mathbf{x}_t . This error leads to lower fidelity in the details of the generated motorcycle.

4.5 Different Initialization

Initialization has a significant impact on the final results. We compare two types of initialization: Point-E and Sphere, and present the results in Figure 6. Guided by the prompt "A military Mech, future, sci-fi", the geometric structure of the final generated results is largely determined by the initialization method. Compared to Sphere, Point-E is able to generate more geometrically detailed results. We also compare the generated results with those from LucidDreamer. With Sphere initialization, our method is somewhat limited in generating the defined feet of the mech, but it produces more detailed features on the body of the military mech. However, with Point-E initialization, our method clearly outperforms LucidDreamer by capturing more complex details.

5 Conclusion

In this paper, we propose a novel approach named Exact Score Matching (ESM), based on Interval Score Matching (ISM), to enhance the consistency during diffusion-based 3D generation processes. Specifically, we first analyze the inherent bias caused by the linear approximation adopted in DDIM, which is unstable and leads to inconsistent generation. To address this issue, we introduce an auxiliary variable and construct an exact recovery algorithm that can alleviate the accumulative error caused by the linear assumption in ISM. Additionally, to effectively and adaptively capture the dynamic changes of the original and auxiliary variables, we leverage LoRA to implement the recovery path. Our overall approach, named ExactDreamer, can be implemented using a single NVIDIA 3090 RTX GPU, and the results demonstrate that ExactDreamer can generate high-fidelity 3D content. However, our methodology does exhibit a few minor limitations, including unstable generation and sensitivity to hyper-parameters, we plan to polish these issues in future improvements. It's also important to acknowledge that while our research is directed towards improving the quality of generative models, it may help in the development of deepfake technology.

References

- [1] Kevin Chen, Christopher B Choy, Manolis Savva, Angel X Chang, Thomas Funkhouser, and Silvio Savarese. Text2shape: Generating shapes from natural language by learning joint embeddings. In *Computer Vision–ACCV 2018: 14th Asian Conference on Computer Vision, Perth, Australia, December 2–6, 2018, Revised Selected Papers, Part III 14*, pages 100–116. Springer, 2019.
- [2] Rui Chen, Yongwei Chen, Ningxin Jiao, and Kui Jia. Fantasia3d: Disentangling geometry and appearance for high-quality text-to-3d content creation. In *Proceedings of the IEEE/CVF International Conference on Computer Vision*, pages 22246–22256, 2023.
- [3] Ming Ding, Zhuoyi Yang, Wenyi Hong, Wendi Zheng, Chang Zhou, Da Yin, Junyang Lin, Xu Zou, Zhou Shao, Hongxia Yang, et al. Cogview: Mastering text-to-image generation via transformers. *Advances in Neural Information Processing Systems*, 34:19822–19835, 2021.
- [4] Haoran Duan, Yang Long, Shidong Wang, Haofeng Zhang, Chris G Willcocks, and Ling Shao. Dynamic unary convolution in transformers. *IEEE Transactions on Pattern Analysis and Machine Intelligence*, 2023.
- [5] Haoran Duan, Shidong Wang, and Yu Guan. Sofa-net: Second-order and first-order attention network for crowd counting. *arXiv preprint arXiv:2008.03723*, 2020.
- [6] Amir Hertz, Ron Mokady, Jay Tenenbaum, Kfir Aberman, Yael Pritch, and Daniel Cohen-Or. Prompt-to-prompt image editing with cross attention control. *arXiv preprint arXiv:2208.01626*, 2022.
- [7] Jonathan Ho, Ajay Jain, and Pieter Abbeel. Denoising diffusion probabilistic models. *Advances in neural information processing systems*, 33:6840–6851, 2020.
- [8] Edward J Hu, Yelong Shen, Phillip Wallis, Zeyuan Allen-Zhu, Yuanzhi Li, Shean Wang, Lu Wang, and Weizhu Chen. Lora: Low-rank adaptation of large language models. *arXiv preprint arXiv:2106.09685*, 2021.
- [9] Nisha Huang, Fan Tang, Weiming Dong, and Changsheng Xu. Draw your art dream: Diverse digital art synthesis with multimodal guided diffusion. In *Proceedings of the 30th ACM International Conference on Multimedia*, pages 1085–1094, 2022.
- [10] Ajay Jain, Ben Mildenhall, Jonathan T Barron, Pieter Abbeel, and Ben Poole. Zero-shot text-guided object generation with dream fields. In *Proceedings of the IEEE/CVF conference on computer vision and pattern recognition*, pages 867–876, 2022.
- [11] Ajay Jain, Amber Xie, and Pieter Abbeel. Vectorfusion: Text-to-svg by abstracting pixel-based diffusion models. In *Proceedings of the IEEE/CVF Conference on Computer Vision and Pattern Recognition*, pages 1911–1920, 2023.
- [12] Heewoo Jun and Alex Nichol. Shap-e: Generating conditional 3d implicit functions. *arXiv preprint arXiv:2305.02463*, 2023.
- [13] Bernhard Kerbl, Georgios Kopanas, Thomas Leimkühler, and George Drettakis. 3d gaussian splatting for real-time radiance field rendering. *ACM Transactions on Graphics*, 42(4):1–14, 2023.
- [14] Gwanghyun Kim, Taesung Kwon, and Jong Chul Ye. Diffusionclip: Text-guided diffusion models for robust image manipulation. In *Proceedings of the IEEE/CVF Conference on Computer Vision and Pattern Recognition*, pages 2426–2435, 2022.
- [15] Mingi Kwon, Jaeseok Jeong, and Youngjung Uh. Diffusion models already have a semantic latent space. *arXiv preprint arXiv:2210.10960*, 2022.
- [16] Bowen Li, Xiaojuan Qi, Thomas Lukasiewicz, and Philip Torr. Controllable text-to-image generation. *Advances in neural information processing systems*, 32, 2019.
- [17] Yixun Liang, Xin Yang, Jiantao Lin, Haodong Li, Xiaogang Xu, and Yingcong Chen. Lucid-dreamer: Towards high-fidelity text-to-3d generation via interval score matching. *arXiv preprint arXiv:2311.11284*, 2023.
- [18] Chen-Hsuan Lin, Jun Gao, Luming Tang, Towaki Takikawa, Xiaohui Zeng, Xun Huang, Karsten Kreis, Sanja Fidler, Ming-Yu Liu, and Tsung-Yi Lin. Magic3d: High-resolution text-to-3d content creation. In *Proceedings of the IEEE/CVF Conference on Computer Vision and Pattern Recognition*, pages 300–309, 2023.

- [19] Shitong Luo and Wei Hu. Diffusion probabilistic models for 3d point cloud generation. In *Proceedings of the IEEE/CVF Conference on Computer Vision and Pattern Recognition*, pages 2837–2845, 2021.
- [20] Ben Mildenhall, Pratul P Srinivasan, Matthew Tancik, Jonathan T Barron, Ravi Ramamoorthi, and Ren Ng. Nerf: Representing scenes as neural radiance fields for view synthesis. *Communications of the ACM*, 65(1):99–106, 2021.
- [21] Alex Nichol, Prafulla Dhariwal, Aditya Ramesh, Pranav Shyam, Pamela Mishkin, Bob McGrew, Ilya Sutskever, and Mark Chen. Glide: Towards photorealistic image generation and editing with text-guided diffusion models. *arXiv preprint arXiv:2112.10741*, 2021.
- [22] Alex Nichol, Heewoo Jun, Prafulla Dhariwal, Pamela Mishkin, and Mark Chen. Point-e: A system for generating 3d point clouds from complex prompts. *arXiv preprint arXiv:2212.08751*, 2022.
- [23] Ben Poole, Ajay Jain, Jonathan T Barron, and Ben Mildenhall. Dreamfusion: Text-to-3d using 2d diffusion. *arXiv preprint arXiv:2209.14988*, 2022.
- [24] Alec Radford, Jong Wook Kim, Chris Hallacy, Aditya Ramesh, Gabriel Goh, Sandhini Agarwal, Girish Sastry, Amanda Askell, Pamela Mishkin, Jack Clark, et al. Learning transferable visual models from natural language supervision. In *International conference on machine learning*, pages 8748–8763. PMLR, 2021.
- [25] Amit Raj, Srinivas Kaza, Ben Poole, Michael Niemeyer, Nataniel Ruiz, Ben Mildenhall, Shiran Zada, Kfir Aberman, Michael Rubinstein, Jonathan Barron, et al. Dreambooth3d: Subject-driven text-to-3d generation. In *Proceedings of the IEEE/CVF International Conference on Computer Vision*, pages 2349–2359, 2023.
- [26] Aditya Ramesh, Mikhail Pavlov, Gabriel Goh, Scott Gray, Chelsea Voss, Alec Radford, Mark Chen, and Ilya Sutskever. Zero-shot text-to-image generation. In *International conference on machine learning*, pages 8821–8831. Pmlr, 2021.
- [27] Scott Reed, Zeynep Akata, Xinchun Yan, Lajanugen Logeswaran, Bernt Schiele, and Honglak Lee. Generative adversarial text to image synthesis. In *International conference on machine learning*, pages 1060–1069. PMLR, 2016.
- [28] Robin Rombach, Andreas Blattmann, Dominik Lorenz, Patrick Esser, and Björn Ommer. High-resolution image synthesis with latent diffusion models. In *Proceedings of the IEEE/CVF conference on computer vision and pattern recognition*, pages 10684–10695, 2022.
- [29] Robin Rombach, Andreas Blattmann, and Björn Ommer. Text-guided synthesis of artistic images with retrieval-augmented diffusion models. *arXiv preprint arXiv:2207.13038*, 2022.
- [30] Nataniel Ruiz, Yuanzhen Li, Varun Jampani, Yael Pritch, Michael Rubinstein, and Kfir Aberman. Dreambooth: Fine tuning text-to-image diffusion models for subject-driven generation. In *Proceedings of the IEEE/CVF Conference on Computer Vision and Pattern Recognition*, pages 22500–22510, 2023.
- [31] Simo Ryu. Low-rank adaptation for fast text-to-image diffusion fine-tuning, 2023. <https://github.com/cloneofsimon/lora>.
- [32] Chitwan Saharia, William Chan, Saurabh Saxena, Lala Li, Jay Whang, Emily L Denton, Kamyar Ghasemipour, Raphael Gontijo Lopes, Burcu Karagol Ayan, Tim Salimans, et al. Photorealistic text-to-image diffusion models with deep language understanding. *Advances in neural information processing systems*, 35:36479–36494, 2022.
- [33] Tianchang Shen, Jun Gao, Kangxue Yin, Ming-Yu Liu, and Sanja Fidler. Deep marching tetrahedra: a hybrid representation for high-resolution 3d shape synthesis. *Advances in Neural Information Processing Systems*, 34:6087–6101, 2021.
- [34] Jiaming Song, Chenlin Meng, and Stefano Ermon. Denoising diffusion implicit models. *arXiv preprint arXiv:2010.02502*, 2020.
- [35] Yang Song, Jascha Sohl-Dickstein, Diederik P Kingma, Abhishek Kumar, Stefano Ermon, and Ben Poole. Score-based generative modeling through stochastic differential equations. *arXiv preprint arXiv:2011.13456*, 2020.
- [36] Jiaxiang Tang, Jiawei Ren, Hang Zhou, Ziwei Liu, and Gang Zeng. Dreamgaussian: Generative gaussian splatting for efficient 3d content creation. *arXiv preprint arXiv:2309.16653*, 2023.

- [37] Bram Wallace, Akash Gokul, and Nikhil Naik. Edict: Exact diffusion inversion via coupled transformations. In *Proceedings of the IEEE/CVF Conference on Computer Vision and Pattern Recognition*, pages 22532–22541, 2023.
- [38] Zhengyi Wang, Cheng Lu, Yikai Wang, Fan Bao, Chongxuan Li, Hang Su, and Jun Zhu. Prolificdreamer: High-fidelity and diverse text-to-3d generation with variational score distillation. *Advances in Neural Information Processing Systems*, 36, 2024.
- [39] Chenfei Wu, Jian Liang, Lei Ji, Fan Yang, Yuejian Fang, Daxin Jiang, and Nan Duan. Nüwa: Visual synthesis pre-training for neural visual world creation. In *European conference on computer vision*, pages 720–736. Springer, 2022.
- [40] Jiajun Wu, Chengkai Zhang, Tianfan Xue, Bill Freeman, and Josh Tenenbaum. Learning a probabilistic latent space of object shapes via 3d generative-adversarial modeling. *Advances in neural information processing systems*, 29, 2016.
- [41] Tao Xu, Pengchuan Zhang, Qiuyuan Huang, Han Zhang, Zhe Gan, Xiaolei Huang, and Xiaodong He. AttnGAN: Fine-grained text to image generation with attentional generative adversarial networks. In *Proceedings of the IEEE conference on computer vision and pattern recognition*, pages 1316–1324, 2018.
- [42] Han Zhang, Tao Xu, Hongsheng Li, Shaoting Zhang, Xiaogang Wang, Xiaolei Huang, and Dimitris N Metaxas. StackGAN: Text to photo-realistic image synthesis with stacked generative adversarial networks. In *Proceedings of the IEEE international conference on computer vision*, pages 5907–5915, 2017.
- [43] Linqi Zhou, Yilun Du, and Jiajun Wu. 3d shape generation and completion through point-voxel diffusion. In *Proceedings of the IEEE/CVF international conference on computer vision*, pages 5826–5835, 2021.